A&A 411, L331–L342 (2003)
DOI: 10.1051/0004-6361:20031440

Astronomy & Astrophysics

Gamma-ray bursts observed by the INTEGRAL-SPI anticoincidence shield: A study of individual pulses and temporal variability⋆

F. Ryde[1], L. Borgonovo[1], S. Larsson[1], N. Lund[2], A. von Kienlin[3], and G. Lichti[3]

[1] Stockholm Observatory, AlbaNova University Center, 106 91 Stockholm, Sweden
[2] Danish Space Research Institute, Juliane Maries vej 30, 2100 Copenhagen O, Denmark
[3] Max-Planck-Institut für extraterrestrische Physik, 85741 Garching bei München, Germany

Received 16 July 2003 / Accepted 16 September 2003

Abstract. We study a set of 28 GRB light-curves detected between 15 December 2002 and 9 June 2003 by the anti-coincidence shield of the spectrometer (SPI) of INTEGRAL. During this period it has detected 50 bursts, that have been confirmed by other instruments, with a time resolution of 50 ms. First, we derive the basic characteristics of the bursts: various duration measures, the count peak flux and the count fluence. Second, a sub-sample of 11 bursts with 12 individual, well-separated pulses is studied. We fit the pulse shape with a model by Kocevski et al. (2003) and find that the pulses are quite self-similar in shape. There is also a weak tendency for the pulses with steep power-law decays to be more asymmetric. Third, the variability of the complex light-curves is studied by analyzing their power-density-spectra (PDS) and their RMS variability. The averaged PDS, of the whole sample, is a power-law with index of 1.60 ± 0.05 and a break between 1–2 Hz. Fourth, we also discuss the background and noise levels. We found that the background noise has a Gaussian distribution and its power is independent of frequency, i.e., it is white noise. However, it does not follow a Poisson statistic since on average the variance is ∼1.6 larger than the mean. We discuss our results in context of the current theoretical picture in which GRBs are created in an anisotropic, highly relativistic outflow from collapsing massive stars. Finally, we note that the exact behaviour of the instrument is not yet known and therefore the above results should be treated as preliminary.

Key words. gamma-rays: bursts – methods: data analysis

1. Introduction

Gamma-ray burst (GRB) light curves are very diverse in morphology. Some only consist of a single, well-shaped pulse, often with a fast rise and a slower decay, while others exhibit very complex and jagged light-curves and, in some cases, long periods of quietness between activity. Various interpretations of the morphologies and the diversity has been proposed within the standard fireball model (Rees & Mészáros 1992), in which an explosive flow of relativistic matter, probably with a large magnetic flux component (Lytikov & Blackman 2001), is released from a central engine and the γ-rays arise from internal shocks within the outflow. The episodic nature of the outflow causes inhomogeneities in the wind (or shells) to collide and thus creating the shocks. Every such emission episode produces a single pulse, which thus is the fundamental constituent of a GRB light curve. More complex light curves are superpositions of several of these (Fishman et al. 1994) and reflect the order in which the shells collide, which depends on the initial energy of the explosion and the distance at which the shocks are optically thin (Kobayashi et al. 2002). The shocks tap the bulk kinetic energy and transform it into random energy of leptons which radiate. The dominant emission mechanisms are most probably non-thermal synchrotron (Tavani 1996; Lloyd & Petrosian 2000) and/or inverse Compton emission (Panaitescu & Mészáros 2000).

The first line of research is therefore to understand the physics of the creation of an individual GRB pulse. There are three main physical time-scales relevant for a pulse: *The curvature timescale* which arises from relativistic effects in a sphere expanding with a high bulk Lorentz factor Γ. Due to the curvature of the shell there will be a time delay between the photons emitted simultaneously in the comoving frame from different points on the surface. Due to the relativistic aberration of light, isotropically emitted radiation in the comoving frame will be beamed into a cone with opening angle $\theta \sim \Gamma^{-1}$. Thus, only photons emitted from the fireball surface within a narrow cone of opening angle $\sim\Gamma^{-1}$ around the line-of-sight will be

Send offprint requests to: F. Ryde, e-mail: felix@astro.su.se

⋆ Based on observations with INTEGRAL, an ESA project with instruments and science data centre funded by ESA member states (especially the PI countries: Denmark, France, Germany, Italy, Switzerland, Spain), Czech Republic and Poland, and with the participation of Russia and the USA.

detectable by the observer. A second time scale is *the cooling time* of the shocked electrons, due to synchrotron and/or inverse Compton losses in radiation and magnetic fields. A simple model scenario for the pulse shape is to assume an impulsive heating of the leptons and a subsequent cooling and emission. The rise phase of the pulse is attributed to the energizing of the shell and the decay phase reflects the cooling and its time scale. Yet another model is one where the pulse duration is set by the *dynamic time* of say the shell crossing, which could be much larger than the microscopic acceleration and/or emission-cooling times. In this case there is a continuous acceleration of particles during shell crossings; the acceleration and the cooling occur in situ and simultaneously and give rise to the observed behavior. The pulse shape then is a reflection of the energizing mechanism of the electrons. As discussed by Ryde & Petrosian (2002) the cooling time is often very short and the two other time scales are comparable in size and dominate over the cooling time.

The second line of research is to try to understand the nature of the complexity or variability of the light curve, for instance, in terms of power at different frequencies and the average difference between the counts and a running mean. Stern et al. (1999) first suggested that there is an intrinsic correlation between the luminosity and the complexity of the burst light-curves. Using GRBs with known redshifts, Fenimore & Ramirez-Ruiz (2000) (see also Reichart et al. 2001) found that the peak luminosities of long bursts are correlated with their gamma-ray variability, V (see Sect. 4 for the definition of V): $L_{\rm iso} \propto V^{3.3^{+1.1}_{-0.9}}$. This correlation, even though tentative, thus gives the possibility to determine, from the variability in the gamma-ray light curve, the *isotropically* equivalent peak luminosity (or luminosity per steradian), i.e., the power output of the burst assuming that the explosion occurs isotropically. It should be stressed that the parameter $L_{\rm iso}$ does not necessarily need to be the actual radiative power output from the burst. If the burst stems from an anisotropic outflow the effective opening angle of such a flow will determine the assigned value of $L_{\rm iso}$ as well. The picture now emerging is that the outflow is indeed anisotropic, i.e. it is collimated and subtends an opening angle, θ much less than 4π (Frail et al. 2001; Panaitescu & Kumar 2001). The total, isotropic energies deduced for burst with known redshifts have a broad distribution. However, by including the information on the opening angle, measured from the break in the afterglow light curve, ($E_{\rm iso}(\theta) = 4E_{\rm corrected}/\theta^2$) the energy distribution narrows significantly, suggesting a near constant energy in the outbursts, narrowly clustered around $E = 10^{51}$ ergs (excluding the efficiency correction). If the explosion energy is near constant then a change in $L_{\rm iso}$, and therefore variability V, depends mainly on θ. V then measures the opening angle which in its turn affects the measured quantity, $L_{\rm iso} \propto L_{\rm const}/\theta^2$. That this correlation exists is shown by Kobayashi et al. (2002) who also suggested an explanation to the observed $V - \theta$ correlation within the internal shock model. They emphasize two main smoothing effects in the multiple shell model both dependent on the bulk Lorentz factor: pair photosphere produced by synchrotron photons at $R_{\pm} \sim 1/\sqrt{\Gamma}$ (see also Zhang & Mészáros 2002) and the angular time scale $\delta t_{\rm ang} \sim R/2c\Gamma^2$. If a collision happens below the photosphere, the whole internal energy produced by the collision is converted to kinetic energy again via the shell spreading. The shells become more ordered and when collisions occur in an optically thin environment the complexity of the light curve will have become smaller than if most collisions occur beyond the pair photosphere. They argue, therefore, that the variability is determined mainly by the bulk Lorentz factor and thus the $V - \theta$ correlation reduces to a $\Gamma - \theta$ correlation, which is reasonable in the collapsar model: the more mass that is entrained in the outflow, which has a near-constant energy, the lower the bulk Γ will be. Numerically they find that the cases, for which data were available, are fitted the best with $\Gamma \propto \theta^{-1}$ and thus the mass loading $M \propto E/(c^2\Gamma) \propto \theta$. Recent observations point towards a connection between GRB and supernovae (Hjorth et al. 2003) which lends additional support to the collapsar description (see, e.g., MacFadyen & Woosley 1999). There are several reasons to believe that such an outflow is indeed collimated.

The power density spectra (PDS) of individual burst are very diverse, and previous studies have shown no clear systematic shape (Giblin et al. 1998). However, assuming that each GRB light curve is a realization of the same stochastic process, Beloborodov et al. (1998, 2000) have shown that the average PDS follows a power-law over 2 frequency decades with an upper cut-off at ∼1 Hz. The power-law index is equal to $-5/3$ within uncertainties, suggesting a connection with the Kolmogorov spectrum of velocities in a turbulent medium.

After shortly describing the instrument in Sect. 2 we present the sample of bursts (Sect. 2.1) and provide plots of all the 28 light curves. We summarize the properties of the various observational parameters, such as durations, count fluences and peak fluxes. In Sect. 3 we study a sub-sample of 11 burst with 12 FRED pulses and finally in Sect. 4 we discuss the bursts in our sample which have complex light curves. We use different types of variability measures.

2. INTEGRAL observations

The INTEGRAL gamma-ray satellite and its instruments are described in Winkler et al. (2003) and references therein. All the instruments onboard INTEGRAL have the capability of observing GRBs located in their field of view (FOV). Six such events have been detected up until June 2003. GRBs from any direction on the sky can also be detected by the anticoincidence shield (ACS) that surrounds the gamma-ray spectrometer, SPI (von Kienlin et al. 2003a). The ACS consists of 91 BGO crystals with a total weight of 512 kg. It has a large effective area for detecting gamma rays but, at least for the initial set-up, provides no directional information for the observed GRBs. The capability to extract some, very crude, directional information might be implemented later on in the mission. The sensitivity and energy threshold for the ACS depends on source direction. Because of the complex structure and design of the ACS the calibration of these properties is still very uncertain. For example, the energy threshold is not constant across the ACS but varies over a wide range. At present the threshold is estimated to 75^{+75}_{-25} keV. A more detailed discussion

Table 1. 28 GRBs observed with the SPI-ACS.

GRB	Time (UTC)	T_{90} (s)	T_{50} (s)	$T_{50}^{\rm em}$ (s)	$T_{f=45}$ (s)	Peak Flux (counts/s)	Fluence (counts)	significance (sigma)	V/E	P/V
20030102	23 : 19 : 00	37 ± 13	5.5 ± 1.5	1.05 ± 0.05	2.3	21 680 ± 90	60 000 ± 7000	26	1.70	
20030105	14 : 34 : 02	13 ± 7	0.4 ± 0.5	0.65 ± 0.05	0.35	53 100 ± 100	37 500 ± 4000	27	1.64	
20030115a	6 : 24 : 30	68 ± 3	33.0 ± 0.3	5.55 ± 0.05	13.2	13630 ± 70	200 000 ± 7000	64	1.61	*V*
20030127	12 : 32 : 32	41.5 ± 0.9	21 ± 2	5.15 ± 0.07	6.65	25 600 ± 300	235 000 ± 15 000	98	1.67	*V*
20030204	12 : 45 : 29	14.0 ± 0.3	7.2 ± 0.4	3.10 ± 0.05	3.65	17 440 ± 40	89 000 ± 3000	62	1.61	
20030217	2 : 45 : 37	50 ± 1	7 ± 2	4.50 ± 0.09	4.05	54 000 ± 1000	370 000 ± 40 000	139	1.45	*PV*
20030218	11 : 42 : 38	67.6 ± 0.8	45 ± 15	2.30 ± 0.06	7.8	54 800 ± 200	430 000 ± 55000	140	1.49	*PV*
20030220	16 : 12 : 43	51 ± 5	29 ± 7	1.6 ± 0.3	11.5	18 100 ± 900	190 000 ± 60 000	71	1.48	*V*
20030223	9 : 45 : 09	14 ± 15	5 ± 1	3.25 ± 0.4	3.9	17 400 ± 750	95 000 ± 30 000	67	1.60	
20030225	15 : 02 : 48	27 ± 10	11 ± 3	1.95 ± 0.5	6.05	11 900 ± 800	75 000 ± 30 000	38	1.48	*P*
20030228	20 : 26 : 47	27 ± 8	11 ± 2	0.70 ± 0.01	11.95	20 450 ± 150	50 000 ± 6000	25	1.69	
20030307	14 : 31 : 58	14 ± 5	1.2 ± 0.1	1.10 ± 0.02	0.85	76 400 ± 400	11 5000 ± 9000	81	1.50	*P*
20030308	5 : 18 : 25	8 ± 15	4 ± 3	1.65 ± 0.1	1.55	15 450 ± 750	36 000 ± 20 000	33	1.53	*PP*
20030320	10 : 11 : 40	57 ± 7	33 ± 0.7	3.3 ± 0.2	8.4	10 500 ± 200	100 000 ± 20 000	35	(1.95)[a]	
20030325	14 : 15 : 14	13 ± 4	1.0 ± 0.9	0.60 ± 0.05	0.7	42 400 ± 400	43 000 ± 7000	31	1.52	*P*
20030329	11 : 37 : 26	19.9 ± 0.6	11.1 ± 0.03	3.25 ± 0.02	3.8	152 200 ± 300	85 5000 ± 10 000	506	1.62	*P*
20030426	23 : 30 : 00	53 ± 16	16 ± 9	2.0 ± 0.2	3.75	20 500 ± 1000	95 000 ± 40 000	34	1.55	
20030505a	7 : 38 : 59	42 ± 6	23.6 ± 0.5	5.35 ± 0.1	8.45	9270 ± 30	100 500 ± 3000	41	1.46	
20030505b	9 : 03 : 22	120 ± 9	94.6 ± 0.1	3.80 ± 0.02	4.3	14 590 ± 30	91 500 ± 6000	22	1.56	*P*
20030506	2 : 04 : 09	30 ± 5	15.4 ± 0.7	8.5 ± 1	9.7	13 000 ± 450	170 000 ± 25 000	84	1.48	*V*
20030509	5 : 50 : 24	6 ± 10	3.9 ± 0.2	0.25 ± 0.05	0.7	90 350 ± 150	70 000 ± 6000	79	1.60	*P*
20030514	18 : 22 : 21	23 ± 9	6 ± 1.5	2.95 ± 0.3	5.05	11 050 ± 400	67 000 ± 15 000	38	1.42	*P*
20030518a	1 : 23 : 45	21.5 ± 1.5	8.7 ± 0.1	6.80 ± 0.02	6.3	51 640 ± 80	486 000 ± 8000	280	1.54	*V*
20030518b	3 : 12 : 18	22 ± 4	10.4 ± 0.9	2.7 ± 0.2	6.25	13 400 ± 350	95 000 ± 12 000	54	1.58	
20030519	9 : 32 : 22	14 ± 13	3 ± 1	0.95 ± 0.04	1.4	15 100 ± 200	30 000 ± 4500	21	1.60	
20030523b	15 : 31 : 02	28 ± 2	13.9 ± 0.6	2.50 ± 0.02	5.85	42 750 ± 250	300 000 ± 15 000	148	1.56	*V*
20030601	22 : 11 : 59	22 ± 8	11 ± 2	4.5 ± 0.4	4.9	17 250 ± 600	120 000 ± 25 000	70	1.55	*V*
20030605a	2 : 19 : 32	76 ± 4	25 ± 10	3.05 ± 0.04	9.25	23 900 ± 850	210 000 ± 80 000	65	1.64	*PV*

[a] Complex background.

of the properties of the ACS with regards to GRBs is given in von Kienlin et al. (2003b).

With the limited knowledge of the calibration of the ACS at this early stage of the mission we will show examples of studies of GRB pulses and temporal variability that can be performed on the large sample of bursts that is being collected by this instrument. In the present paper we have studied the 28 strongest bursts observed by the time of writing. The available light curves has a time resolution of 50 ms and the ACS is expected to detect some 300 GRBs or GRB candidates per year.

2.1. GRB light curves and the sample selection

Events which trigger the IBAS with a significance of at least 6 sigma are screened for solar flares and X-ray flares to single out possible GRB candidates. This threshold has been chosen because several bursts, triggered with such a significance, have been confirmed later as GRBs by the interplanetary network (IPN). The triggers and alerts are sent by the IBAS alert system managed by the ISDC (Mereghetti et al. 2003; Courvoisier et al. 2003). The SPI-ACS has recorded 149 such events until 9 June 2003, of which 50 are confirmed as GRBs with 6 detected in the field of view of the IBIS and/or SPI. We calculated the significance, S, as the number of sigmas above the background for these 50 bursts. We used the criterion $S > 20$ to allow a burst to be included in our sample. We thereby dismiss bursts that are too noisy to give useful results in our analysis. We also do not include very short bursts, e.g. spikes. The resulting 28 bursts are listed in Table 1 where we give date and time in UTC for each burst. The light curves are shown in Fig. 1. Here the original time resolution is used and the flux is given as counts per 50 ms time bin. Note that these light curves are not background subtracted and thus the background level can be seen. For every burst, the background is modeled with a polynomial function (mainly of first order, with a few second order fits) in time and subtracted from the count data. The maximal value of the count rate, on the 50 ms times-scale, is then determined as well as the total count fluence over T_{90} (see below for a definition). Together with these values in Table 1 are various measures of the light-curve duration. A well defined duration is an important physical quantity, both when it comes to study cosmological time dilation effects as well as to discern characteristic time scale for the mechanism giving rise to the radiation. We will estimate the duration of the

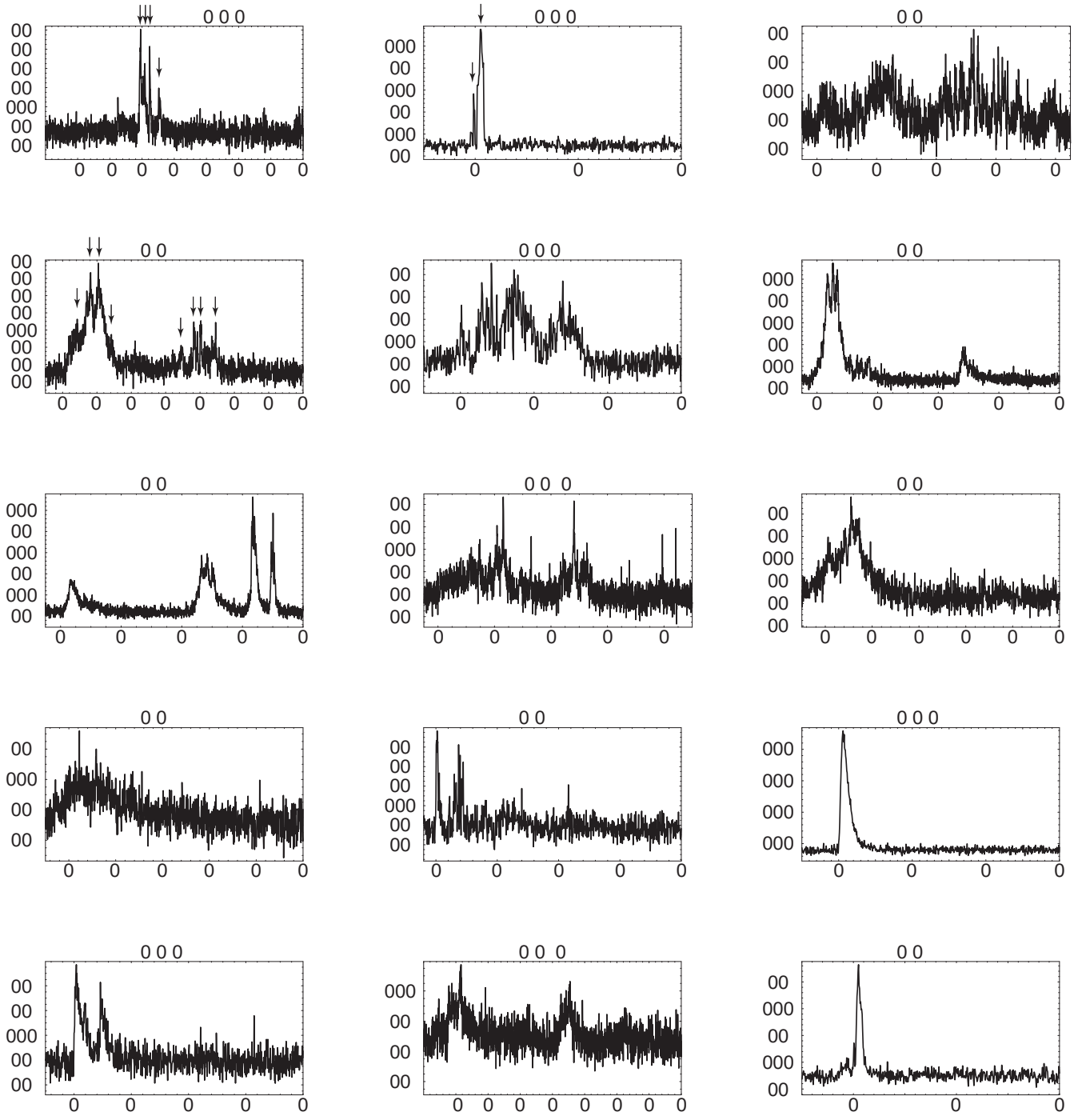

Fig. 1. INTEGRAL SPI anticoincidence-shield light-curves as counts per time bin, with a time resolution is 50 ms. The bursts were observed from 15 December 2002 until 9 June 2003 and only the bursts with highest significance are displayed and used in the presented study. GRB 030329 has a known redshift of $z = 0.1685$.

bursts by measuring T_{50} and T_{90} which are the time scales over which 50% and 90%, respectively, of the radiation is emitted. Such measures are not useful in cases where there are long periods of quietness in the light curve, a phenomenon which is very often seen in GRB light curves. We therefore also provide other duration measures: *the emission time* $T_{50}^{\rm em}$, which is the summed time for which the bursts has emission that is stronger than 50% of the peak flux level, see e.g. Bonnell et al. (1997) and $T_{f=0.45}$, which is the summed time over which the most intense fraction f of the total flux is emitted. The reason for choosing $f = 0.45$ is given in Sect. 4.

The background emission is in most cases very well-behaved and is fairly constant. A first order polynomial provides, in general, a good fit. However in a few cases, the temporal proximity of other transients, e.g. solar flares, make the background estimation more difficult. From analyzing the

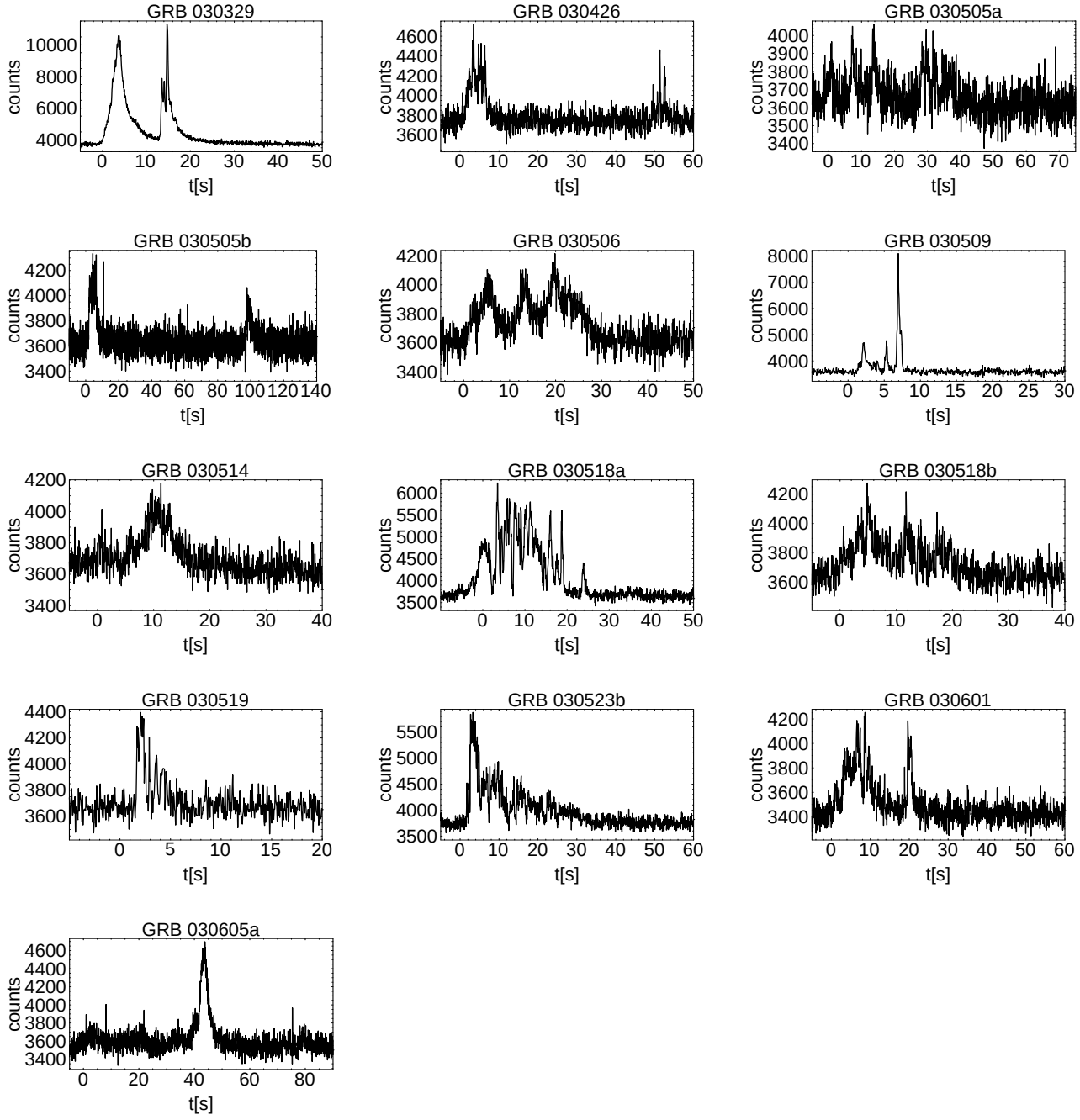

Fig. 1. continued.

power density spectrum (PDS; see Sect. 4.1) and from the analytical fitting of the individual pulses (see Sect. 3) it is apparent that the variance in the observations are larger than expected for simple counting (Poissonian) statistics. The normalized background-noise distribution for a typical case (GRB 030307, see Fig. 1) is shown in Fig. 2. The inset shows the time interval used to study the background noise. A Gaussian fits the distribution very well (which is expected for a Poissonian process with a large expectation value or mean). Using the Geary test (Devore 1982) and assuming that the distribution is normal as the null hypothesis, the *P*-value is 0.93 and therefore we accept the hypothesis with very high confidence. The *P*-value is the probability that the value of the test statistic is as extreme as it is, with the null hypothesis being true. However, we note that the variance is not equal to the mean number of counts per bin which is expected for Poissonian noise. However, the ratio between the mean and the variance is approximately constant from case to case as is indicated in Table 1. These ratios were computed from post-burst background data for each burst, similarly as shown in Fig. 2. The next question that arises is then if the burst signal has the same behavior as the background. Since the cause of the increased variance is still unclear we do not know if it affects events produced by both photons and particles in the same way. The pulse analysis and the power density spectrum studies in the following sections are not conclusive, but produce more consistent results if the signal variance is also

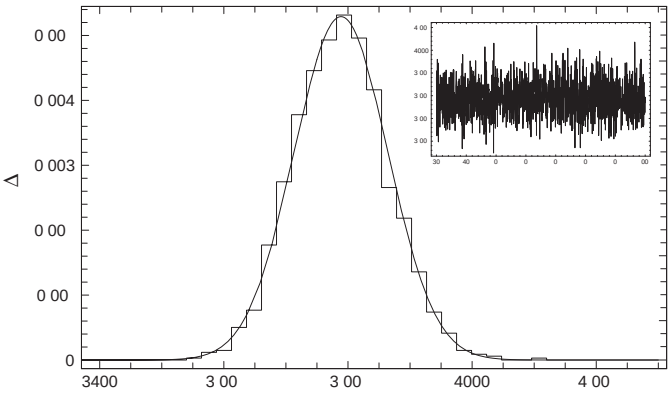

Fig. 2. Normalized histogram of the distribution of the background counts for GRB 030307 (see Fig. 1). The inset shows the time interval (70 s), well after the burst proper without any obvious burst activity, used to study the background. The noise has a Gaussian distribution (which is expected for a Poissonian process with a large expectation value or mean). However, the mean value $\mu = 3789$ and the standard the deviation is $\sigma = 75.4$ (i.e., a variance $\sigma^2 = 5687$). Since the difference between mean and variance is highly significant, the background noise is not Poissonian.

assumed to be larger than Poissonian by the same factor. For all statistical analysis in this paper the noise variance is estimated by multiplying the expected Poissonian noise with a constant factor determined from the background data. A more detailed investigation of this effect is being performed by the hardware group of MPE.

3. Pulses

In general, GRB pulses are asymmetric with a fast rise and a slower decay. The current understanding of the shape of the pulse is based on the knowledge of the spectral evolution. The complete spectral and temporal evolution of a pulse can be characterized by three main observables, the peak of the energy spectrum, $E_{\rm p}(t)$, the instantaneous energy flux, $F(t)$, and the derived quantity, the energy fluence $\mathcal{E}(t) = \int^t F{\rm d}t'$. The relations between these three observables are given by two empirical correlations:

(i) the hardness-intensity correlation (HIC; Golenetski et al. 1983), which relates the flux of the source to the "hardness" of the spectrum (here represented by $E = E_{\rm p}$). For the decay phase of a pulse the most common behavior of the HIC is

$$F = F_0(E_{\rm p}/E_{\rm p,0})^{\eta}, \tag{1}$$

where $E_{\rm p,0}$ and F_0 are the initial values of the peak energy and the energy flux at the beginning of the decay phase in each pulse and η is the power law index.

(ii) the hardness-fluence correlation, $E_{\rm p}(\mathcal{E})$ (HFC; Liang 1997; Liang & Kargatis 1996) which relates the hardness to the time running integral of the flux, i.e. the fluence. Equivalently, the HFC represents the observation that the rate of change in the hardness is proportional to the luminosity of the radiating medium (or, equivalently, to the energy density);

$$\dot{E} = -\frac{F}{\phi_0}\cdot \tag{2}$$

Using the energy flux, F, this corresponds to a linear relation between the $E_{\rm p}$ and the time integrated energy flux, the energy fluence

$$E_{\rm p}(t) = E_{\rm p,0} - \frac{\mathcal{E}(t)}{\Phi_0} \tag{3}$$

where Φ_0 is the decay constant. This behavior is most often seen over the entire pulse. Combining these correlations and by studying light curves during pulse decay phases Ryde & Svensson (2000) have shown that the observed photon flux, $F(E)/E$ or $F(\nu)/\nu$, can often be described by a reciprocal function in time. Ryde et al. (2003) derived the corresponding decay shape for the bolometric energy flux ($F_{\rm bol}$), which in general can be described by

$$F_{\rm bol}(t) = F_{\rm bol,0}\left(1 + \frac{t}{\tau}\right)^{-d}. \tag{4}$$

The evolution of $E_{\rm p}$ is still from hard to soft during the main part of the *rise phase* of a pulse. The energy flux and the $E_{\rm p}$ are thus anti-correlated during the rise phase. By arguing from physical first principles Kocevski et al. (2003) studied several analytical shapes for the whole pulse that includes the rise phase and asymptotically approaches Eq. (4) in the decay phase: in most physical models both the peak of the energy spectrum and the luminosity are proportional to the random Lorentz factor of the shocked electrons to some power: $E_{\rm p}(t) \propto \Gamma_{\rm r}^a(t)\cdot g(t)$, and $F_{\rm E}(t) \propto \Gamma_{\rm r}^b(t)\cdot h(t)$. The functions $g(t)$ and $h(t)$ parameterize the unknown time dependencies on particle densities, optical depth, magnetic field, kinematics, etc. The correlation between hardness and the energy flux can thus be described as

$$F_{\rm E}(t) \propto E_{\rm p}^{\gamma}\cdot f(t) \tag{5}$$

with $\gamma = b/a$ and $f(t) = h(t)g(t)^{-\gamma}$. During the decay phase of a pulse the power law relation dominates the HIC which has been manifested in previous studies. However, the HIC during the rise phase will be dominated by the unknown function $f(t)$. Kocevski et al. (2003) found that the prescription that fitted the best (using an extensive sample of pulses observed by BATSE on *CGRO*) was $f(t) \propto t^r$ where the power law index r represents the rise. They introduced two new parameters, the energy flux and the time of the peak of the light curve, $F_{\rm m}$ and $t_{\rm m}$:

$$F = F_{\rm m}\left(\frac{E_{\rm p}}{E_{\rm m}}\right)^{\gamma}\left(\frac{t}{t_{\rm m}}\right)^{r} \tag{6}$$

which combined with the HFC gives the differential equation governing the spectral and temporal evolution of the pulse. It has the following solution (see Kocevski et al. 2003).

$$\frac{F}{F_{\rm m}}(t) = \left(\frac{t}{t_{\rm m}}\right)^{r}\left(\frac{d}{d+r} + \frac{r}{d+r}\left(\frac{t}{t_{\rm m}}\right)^{r+1}\right)^{-\frac{r+d}{r+1}}, \tag{7}$$

where we have defined the exponent d (for finite r) to describe the asymptotic power law behavior of the light curve, $F(t) \rightarrow t^{-d}$ as $t \rightarrow \infty$ which gives $\gamma = (d+r)/(d-1)$. Equation (7) describes the GRB pulse shape by two parameters, r and d apart from the position of the peak, $F_{\rm m}, t_{\rm m}$.

In the present study, we have selected a sub-sample of the bursts in Table 1 (denoted by a *P*) that contain clear and well-separated pulses, and model them with Eq. (7). In Table 2 the results of the modeling are shown; the time for the peak of the pulse, $t_{\rm max}$, and the power law indices, r and d as well as the full width at half maximum ($FWHM$). Fits to two pulses in the sample (GRB 030217 and GRB 030307) are shown in Fig. 4 as an illustration. Note that these have been rebinned from the original time scale to improve clarity.

Assuming pure Poisson noise for both the background and burst signal the reduced χ^2-values of the fits cluster around 1.6. As the fits are visually good (see e.g. Fig. 4) this suggests that such an assumption underestimates the true noise, leading to a larger χ^2 value. Therefore, we assume that the variance of signal is $V/E \times C_{\rm bin}$, where $C_{\rm bin}$ is the number of counts in a time-bin and V/E is the ratio of the measured variance and mean of a section of burst-free, post-burst background, and indicated for every burst in Table 1. The averaged χ^2 value for the sample is then $\langle\chi^2\rangle = 1.31 \pm 0.34$, by using this estimation of the variance. See further discussion on the noise in Sect. 4.

To study the general behavior of the pulses we calculate a few characteristics from the analytical fits to the data, beside the $FWHM$ and r, and d. First, we find the full width at a tenth of the pulse maximum. This gives a reasonable estimate of the duration of the whole pulse. Then we calculate the rise time, $\tau_{\rm r}$ and the decay times $\tau_{\rm d}$, which are defined as the time from the beginning of the above time interval to the peak time, $t_{\rm max}$ and from $t_{\rm max}$ to the end of that time interval. We then define the pulse asymmetry, PA as being the ratio between the rise time and the decay time:

$$PA = \frac{\tau_{\rm r}}{\tau_{\rm d}}. \qquad (8)$$

Some of the relations between the characteristics are depicted in Fig. 5. Panel (a) shows the very good correlation between the rise time, $\tau_{\rm r}$ and the $FWHM$ of the pulse in the sample. The slope of the linear fit is 0.58 ± 0.02 and the linear correlation coefficient is $R = 0.994$. Such a correlation is demonstrated in the BATSE data as well by Kocevski et al. (2003). Panel (b) shows a similar correlation for the decay time, but with less significance ($R = 0.942$). Here the slope is 1.6 ± 0.2. This is also manifested in Panel (c) which shows that there is no significant trend or correlation between the pulse asymmetry and the width of the pulse. However, there is a significant spread with asymmetry ranging from 0.3 to 0.62. Finally the relation between the rise time and the decay time is not either very strong with $R = 0.907$. The slope here is 0.31 ± 0.04.

In Fig. 6 the change in pulse shape as a function of the decay power-law index d is illustrated. In panel (a) d is plotted versus the normalized rise-time ($\tau_{\rm r}/FWHM$), while in panel (b) the pulse asymmetry ($\tau_{\rm r}/\tau_{\rm d}$) is plotted against the d value. Both these correlation are weak (for a: $R = 0.86$ and for b: $R = 0.97$) but there is a trend that for large d values ($d > 2$) the rise time constitutes a larger fraction of the pulse (a) and equivalently that the pulses are more symmetric (b).

The averaged value of the d parameter is $\langle d\rangle = 2.37 \pm 0.27$ with a standard deviation of 0.95. We note that five cases (40%) are within a few σ of the value 2 with two case at very low values around 1 and another five cases between ~3 and 4. The corresponding values for r is $\langle r\rangle = 2.6 \pm 0.4$ with a standard deviation of 1.4.

Table 2. 12 pulses in 11 GRBs.

GRB	$t_{\rm max}$ (s)	r	d	$FWHM$ (s)
20030217	48.280 ± 0.003	2.21 ± 0.01	2.01 ± 0.01	3.199 ± 0.004
20030218	3.50 ± 0.04	6 ± 1	1.85 ± 0.09	4.88 ± 0.06
20030225	3.15 ± 0.1	1.70 ± 0.06	3.4 ± 0.15	13.90 ± 0.15
20030307	0.639 ± 0.005	1.48 ± 0.09	2.84 ± 0.08	1.140 ± 0.007
20030308	0.39 ± 0.01	1.06 ± 0.08	1.13 ± 0.05	1.35 ± 0.02
20030308	5.02 ± 0.03	2.1 ± 0.2	2.1 ± 0.15	1.51 ± 0.04
20030325	0.491 ± 0.007	1.5 ± 0.5	4.0 ± 0.5	0.54 ± 0.01
20030329	3.559 ± 0.005	3.2 ± 0.5	1.82 ± 0.04	2.200 ± 0.006
20030505	98.51 ± 0.06	2.8 ± 0.3	1.69 ± 0.09	3.47 ± 0.09
20030514	10.380 ± 0.006	3.02 ± 0.01	3.15 ± 0.01	5.700 ± 0.009
20030509	2.08 ± 0.01	2.5 ± 4	1.1 ± 0.2	0.57 ± 0.015
20030605	43.22 ± 0.02	4.0 ± 0.5	3.3 ± 0.15	3.39 ± 0.04

The pulse asymmetry for the sample is $PA = 0.22 \pm 0.11$. If one, alternatively, uses a definition of the asymmetry as the fraction of the $FWHM$ that is before and after $t_{\rm max}$, then $PA = 0.49 \pm 0.11$.

4. Variability

In this section we study the variability of the complex bursts, listed in Table 1, that are denoted by V in the last column. We calculate their power density spectra, their root mean square variability as well as the number of pulses they include.

4.1. Power Density Spectrum, PDS

The power density spectrum P_j of a discrete signal x_k with N uniform time bins is defined as the square of the absolute value of its Fourier transform a_j, for which we used the definition

$$a_j = \sum_{k=0}^{N-1} x_k {\rm e}^{2\pi {\rm i} jk/N}, \quad j = -\frac{N}{2}, \ldots, \frac{N}{2} - 1. \qquad (9)$$

As we discussed in Sect. 1, previous PDS analyses of burst data, taken from BATSE, did not revealed any general trait. Our sample of the INTEGRAL bursts shows the same diversity of PDS shapes, therefore, we did a statistical analysis to look for general trends.

To calculate an average PDS the GRB light curves have to be normalized to make them independent of their intensity. We followed Beloborodov et al. (1998), where it was found that the peak count rate normalization minimizes the average PDS fluctuations. We selected a sample of 10 bursts with a time duration $t_{90} > 20$ s and signal significance $>60\sigma$ (see bursts marked in Table 1 with V). Another important consideration is the noise

subtraction. The Poisson noise due to the counting process, that in general appears as a flat high-frequency component, is usually easily estimated on each individual PDS because its level is given by the fluence (including the background) of the burst. From Parseval's theorem

$$\sum_{k=0}^{N-1} |x_k|^2 = \frac{1}{N} \sum_{j=-N/2}^{N/2-1} |a_j|^2, \tag{10}$$

it follows that the variance Var(x) is given by

$$(N-1)\mathrm{Var}(x) = \frac{1}{N} \sum_{j=-N/2;\ j\neq 0}^{N/2-1} |a_j|^2, \tag{11}$$

and since for a Poisson distribution the variance is equal to the mean $\langle x_k \rangle$, the fluence $\sum x_k = N\langle x_k \rangle \simeq \langle P_j \rangle$ will give the average level of the Poisson noise. The frequency-independent, flat shape of its spectrum derives from the uncorrelated nature of the counting fluctuations. But dead-time of the instrument, additional noise components, scaling, and other effects can produce significant deviations from the expected Poisson distribution. The variance and mean values of the background signal before and after each burst can be directly calculated and their ratios, listed in Table 1, show that there is a substantial noise broadening. Yet, in the example shown in Figs. 2 and 3 we can see that the background noise spectrum is flat and that its amplitude distribution is fairly Gaussian. The next question is whether the burst photon signal is biased in the same way as the background signal. If it is an instrumental effect, then we would expect the same deviation for both signals. On the other hand, if there is a non-Poissonian background noise component due to particle flux, this should not affect the Poisson counting of the photons independently of the source. We tried various estimations of the total noise based on these different assumptions, but the results differ on how steep the high end cut-off is, and do not affect significantly the rest of the spectrum. In Fig. 7 we show the average PDS with and without noise subtraction. For the figure the noise was assumed to be 1.6 of the fluence, approximately the noise level found for the background (see Table 1). A power-law fit gave an index 1.60 ± 0.05, i.e., an approximately Kolmogorov power-law and a cut-off between 1–2 Hz, in agreement with previous studies.

4.2. rms variability

To quantify the variability, or spikiness, of the pulse profiles we use a measure introduced by Fenimore & Ramirez-Ruiz (2000) and later modified by Reichart et al. (2001). The variability is computed from the variance of the light-curve with respect to a smoothed version of itself. The smoothing is performed by applying a box-car filter function. We choose the smoothing time scale to be $T_{f=0.45}$, which was shown to be the best time scale by Reichart et al. (2001). This is the effective time for which the integrated flux under the brightest parts of the burst is 45% of the total flux. Reichart et al. (2001) also took into account time dilation and the narrowing of pulses with increasing energy. In this preliminary analysis we make a correction for the noise level, but leave $z = 0$ and compute the variability for the sample in Table 1. The results are presented in Table 3. The variance of the noise is assumed to be 1.57 of the mean value, as discussed above.

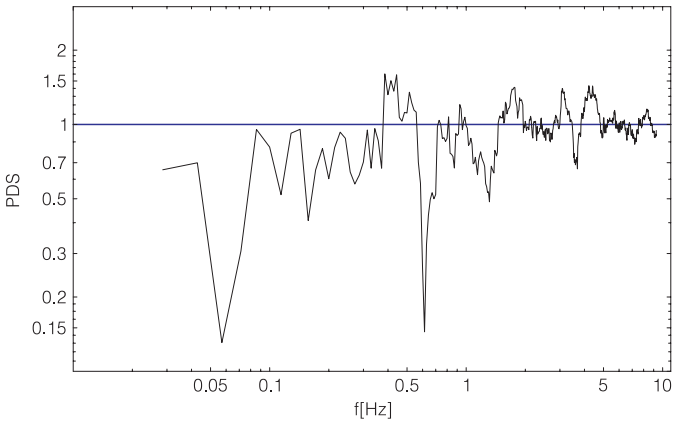

Fig. 3. Power density spectrum (PDS) of the background noise for GRB 030307, see also Fig. 2. The PDS fluctuations have been smoothed on a scale of $\Delta \log f = 0.03$, and the variance was used for normalization. The overall spectrum is flat, as it is characteristic in *white* noise.

Table 3. Variability of the sample.

GRB	Variability	No. of pulses
20030102	0.28 ± 0.03	4
20030105	0.082 ± 0.007	2
20030115a	0.29 ± 0.02	5–15
20030127	0.084 ± 0.006	8
20030204	0.17 ± 0.02	4
20030217	0.045 ± 0.002	9
20030218	0.370 ± 0.007	8
20030220	0.23 ± 0.02	11
20030223	0.03 ± 0.01	2
20030225	0.05 ± 0.03	1
20030228	0.63 ± 0.07	3–6
20030307	0.022 ± 0.002	1
20030308	0.12 ± 0.03	2
20030320	0.12 ± 0.05	4
20030325	0.07 ± 0.01	2
20030329	0.100 ± 0.002	3
20030426	0.13 ± 0.02	6
20030505a	0.24 ± 0.05	7
20030505b	0.09 ± 0.04	2
20030506	0.07 ± 0.02	6
20030509	0.17 ± 0.01	5
20030514	0.02 ± 0.02	1
20030518a	0.168 ± 0.003	20
20030518b	0.11 ± 0.03	7
20030519	0.21 ± 0.04	3
20030523b	0.23 ± 0.01	13
20030601	0.15 ± 0.02	6
20030605a	0.20 ± 0.02	1

As an alternative variance measure we also count the number of pulses. This is done by eye, which has the advantage of not introducing any biases from the de-noising techniques and

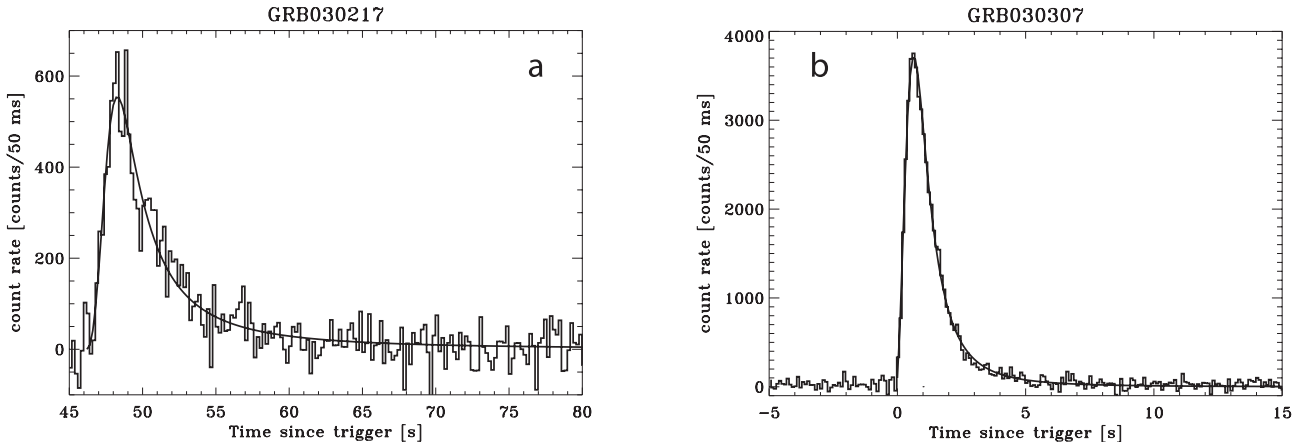

Fig. 4. Fits of the analytical model in Eq. (7) to pulses in GRB 030212 (panel **a)**) and GRB 030307 (panel **b)**). Note that the light curves have been rebinned to a time resolution of 0.2 s for GRB 030212 and 0.1 s for GRB 030307.

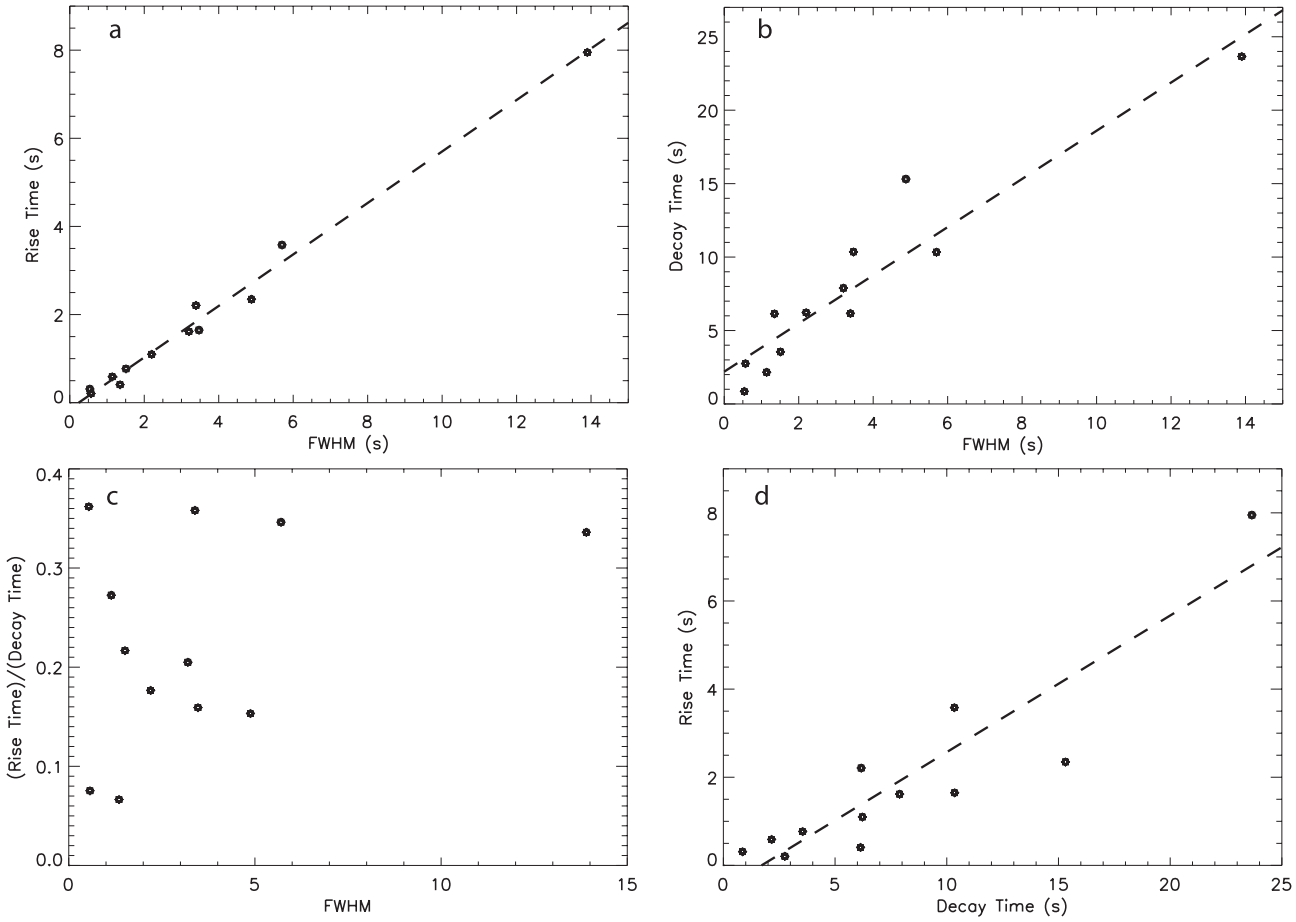

Fig. 5. a) Rise time versus the $FWHM$ of the 12 pulses in our pulse sample (see Table 2). A strong correlation exists with a slope of 0.58 ± 0.02 and a $R = 0.994$. **b)** Decay time of the pulses versus their $FWHM$ values. A larger scatter gives a less significant correlation ($R = 0.942$). The best linear fit has a slope of 1.6 ± 0.2. **c)** Pulse asymmetry (rise time/decay time) versus the width of the pulses ($FWHM$) showing no strong correlation ($R = 0.38$). **d)** Rise time versus decay time. $R = 0.907$ and the best linear fit slope is 0.31 ± 0.04.

pulse identification methods. On the other hand the method is somewhat subjective and the result should be interpreted with caution. The counts were made in plots of higher resolution than those in Fig. 1. A few examples of pulse identifications are indicated in the figure. These results is also given in Table 3. The relation between the variability measure and the number of pulses is shown in Fig. 8. Although the dispersion is large and the relation gives a low linear correlation coefficient, $R = 0.23$, statistically, a larger variability does corresponds to a larger number of pulses. The Spearman rank test gives a correlation coefficient $R_s = 0.46$ with a P-value 0.008 of the *non-linear* correlation being by chance.

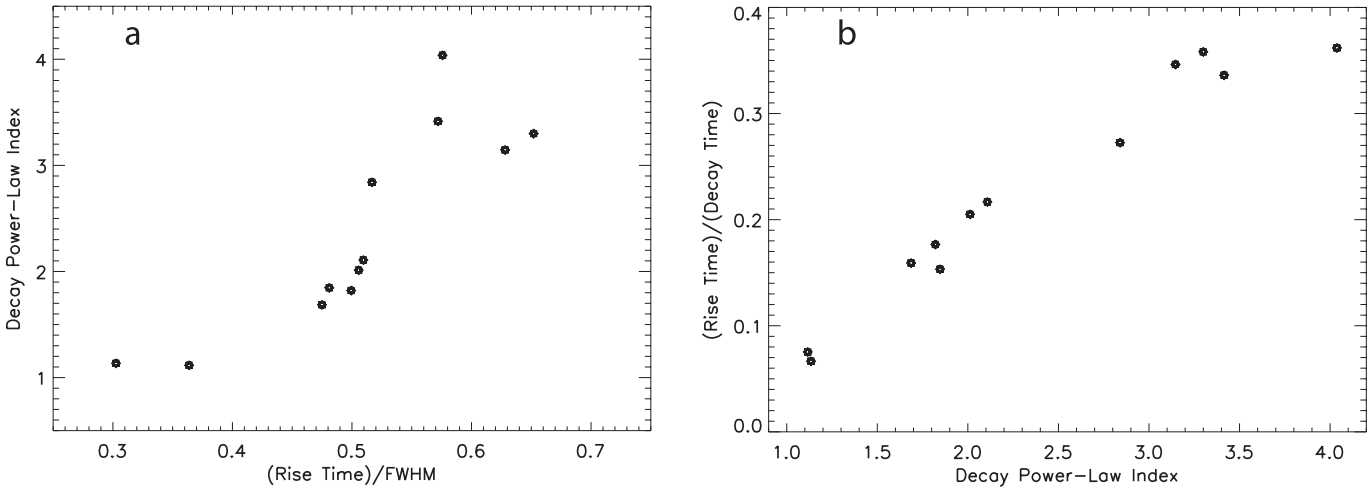

Fig. 6. a) Decay power-law index, d (defined in Eq. (7)), versus the normalized rise time. The correlation has $R = 0.86$. **b)** Pulse asymmetry (Eq. (8)) versus the decay power-law index d (Eq. (7)). There is a weak trend ($R = 0.97$) that pulses with higher d-values are more symmetric.

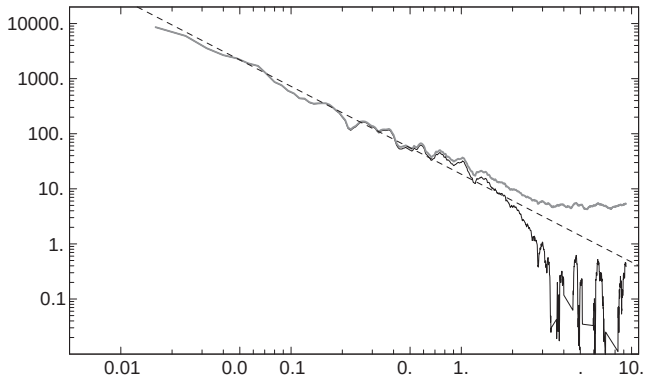

Fig. 7. Average PDS without noise subtraction (gray line) and with noise subtracted (solid line). Fluctuations have been smoothed on a scale of $\Delta \log f = 0.03$. The best fit power-law slope is 1.60 ± 0.05 (power-law fit dashed line). After removing the noise level (dashed curve) a break in the PDS is revealed at 1–2 Hz (somewhat dependent on the background subtraction).

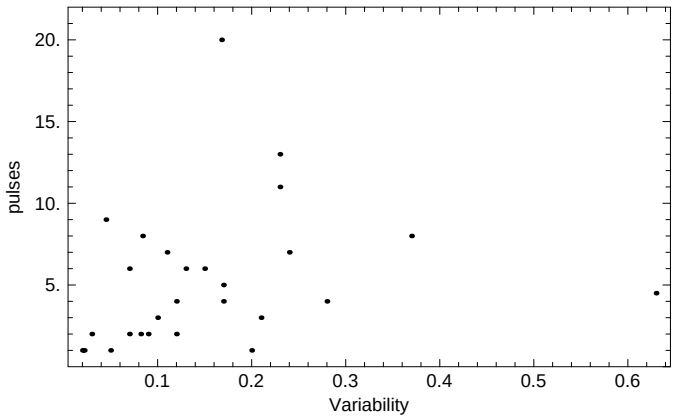

Fig. 8. Relation between the variability measure and the number of pulses. The linear correlation coefficient is $R = 0.23$ and the Spearman rank test gives a correlation coefficient $R_s = 0.46$ with a P-value 0.008 of the correlation being by chance.

5. Discussion

We want to stress again that at this early stage of the mission, we still have limited knowledge of the calibration of the ACS and that there are open issues and problems which have to be solved in near future. The analysis of the burst variability and pulse shapes presented above should, therefore, be judged in the light of these uncertainties and are therefore preliminary.

5.1. Pulses

If the dynamical time-scale and the curvature time-scale of an individual emission-episode, are of the same order, then a pulse will be the convolution of the comoving, intrinsic pulse and the curvature effect (Ryde & Petrosian 2002). The rise phase will roughly be set by the dynamical time and the decay time will be largely affected by the curvature time-scale. The tendency in Fig. 5d suggests that, if the curvature time-scale is important, it is of the same order as the dynamical time scale. Asymptotically, i.e. at late times the light curve will reveal a power-law behavior with an index of 2. In the sample studied above approximately 40% of the cases are consistent with this. There is a tendency in Fig. 6b, that high values of d are associated with more symmetric pulses. By interpreting these cases as being dominated by the dynamical time (compared to the curvature time) the effect of the curvature will be smaller and the intrinsic pulse behavior is more revealed. For cases around 2, however, the asymmetry is more pronounced.

The correlations in Fig. 5 also suggest that the pulse asymmetry varies little from pulse to pulse and is independent of pulse duration and intensity.

Note that this study only includes long pulses and no spikes. Furthermore, it is common in other works to not only study free-standing pulses but rather to use pulses identified by disentangling complicated light-curves, with heavily overlapping pulses. The conclusion from this analysis is that the pulses are remarkably self-similar, independent of their

duration and amplitude. This was also noted for BASTE pulses by Kocevski et al. (2003).

5.2. PDS and variability

The preliminary results on the PDS analysis presented here are based on a small sample and the fact that we found a power-law index slightly larger than Beloborodov et al. (1998) is not significant. Furthermore, Beloborodov et al. (2000), who analyzed the average PDS for three luminosity classes, found that dimmer bursts have on average steeper PDS. Therefore, since our sample belongs to the brightest class, one should expect more high frequency emission and a less steep slope. Chang et al. (2002) found a weak anticorrelation between the power-law index and redshift, which is in agreement with that work, although the luminosity function of GRBs is known to be very broad. Lazzati (2002) has shown that the variability measure is strongly correlated with the frequency that contains most of the power in the burst comoving frame, and therefore it is also a luminosity indicator. Unfortunately, at this point there is only one INTEGRAL burst with known redshift, so it will remain for future work to calibrate these important empirical relations for ACS-SPI data.

To be able to correlate the variability measure with physical quantities (e.g. opening angles and $L_{\rm iso}$) the distance scale has to be measured. There are a few cases for which there are redshift measurements attached. This has only been possible during the past few years with the advent of quick optical follow-up observations. Such observations settles the distance to these bursts and therefore their luminosity. Approximately 35 redshift estimates of bursts have been made. In our sample only the redshift of GRB 030329 is known ($z = 0.1685$ and is suggested to be connected to SN 2003dh by, e.g., Hjorth et al. 2003), and thereby the isotropic luminosity, $L_{\rm iso}$. To be able to calibrate the variabilities measured by INTEGRAL, we therefore have to wait for further measurements of redshifts of INTEGRAL bursts. With the frequency of this to happen increasing, especially with the advent of the *Swift* mission, this will be possible in the near future.

5.3. Counts

It should be noticed that in the analysis made here the light curves were in counts and not energy flux. Assuming no spectral evolution during the pulse, there would be a constant correspondence between the count rate and the photon flux in the same energy range. For a burst with a different spectrum, the constant would be different. However, significant spectral evolution does take place during pulses (see, e.g., Ryde 1999) and therefore the count-rate light-curve could result in a misleading interpretation.

The GRB spectrum is often peaked in the νF_ν representation (where F_ν is the energy flux) at some energy $E_{\rm p}$ in the gamma-ray band. The "bolometric correction" will mainly be dependent on $E_{\rm p}$, i.e., the evolution of the spectrum in the observed energy band. Borgonovo et al. (2003) studied this for BATSE bursts and compared the energy flux F with the count rate C for cases where the $E_{\rm p}$ is known with high temporal resolution. They found that the average bolometric correction, as a function of $E_{\rm p}$, can be described by a second-order polynomial. Furthermore, the energy flux F is in general correlated with $E_{\rm p}$ through the hardness-intensity correlation (Eq. (1)), $F \propto E_{\rm p}^{\eta}$ where the distribution of the parameter η peaks at 2.0 and has a somewhat broad dispersion. Combining the HIC with the general relation discussed above, one would therefore expect a relation between count rate C and energy flux F for individual pulses. Empirically, Borgonovo et al. (2003) found that for BATSE the energy flux is described by a power law of the count rate for individual pulses. The distribution of the power-law index is quite narrowly peaked around 1.2 but stretches between 0.7 and 1.8. Therefore the count-rate curves are good approximations of the energy-flux light-curves in most cases. However, the distribution shows that there are a number of cases for which a correction must be made. A corresponding study should be made on INTEGRAL bursts as well to validate the interpretations of the count-light curves.

Acknowledgements. We are grateful for the support of the INTEGRAL Science Data Centre (ISDC) in Geneva, and to Swedish National Space Board.

References

Beloborodov, A. M., Stern, B. E., & Svensson, R. 1998, ApJ, 508, L25
Beloborodov, A. M., Stern, B. E., & Svensson, R. 2000, ApJ, 535, 158
Bonnell, J. T., Norris, J. P., Nemiroff, R. J., & Scargle, J. D. 1997, ApJ, 490, 79
Borgonovo, L., Ryde, F., & de Val Borro, M. 2003, in Proc. Gamma-Ray Bursts in the Afterglow Era: 3rd Workshop, 17–20 September 2003, in press
Borgonovo, L., Ryde, F., de Val Borro, M., & Svensson, R. 2003, in AIP Conf. Proc. 662, Gamma-Ray Bursts and Afterglow Astronomy 2001, ed. G. R. Ricker, & R. K. Vanderspek, (New York: AIP), 264
Chang, H.-Y., Yoon, S.-J., & Choi, C.-S. 2002, A&A, 383, L1
Courvoisier, T. J. -L., Walter, R., Beckmann, V., et al. 2003, A&A, 411, L53
Devore, J. L. 1982, Probability and Statistics for Engineering and the Sciences (1st ed.; Monterey: Brooks/Cole Publishing Company)
Fenimore, E. E., & Ramirez-Ruiz, E. 2000, ApJ, submitted [astro-ph/0004176]
Fishman, G. J., Meegan, C. A., Wilson, R. B., et al. 1994, ApJS, 92, 229
Frail, D. A., Kulkarni, S. R., Sari, R., Djorgovski, S. G., et al. 2001, ApJ, 562, L55
Giblin, T. W., Kouveliotou, C., & van Paradijs, J. 1998, Gamma-Ray Bursts, 4th Hunstville Symp., 241
Golenetskii, S. V., Mazets, E. P., Aptekar, R. L., & Ilyinskii, V. N. 1983, Nature, 306, 451
Hjorth, J., Sollerman, J., Møller, P., et al. 2003, Nature, 423, 847
von Kienlin, A., Arend, N., Lichti, G. G., Strong, A. W., & Connell, P. 2003, Proc. SPIE, 4851, 1336
von Kienlin, A., Beckmann, V., Rau, A., et al. 2003b, A&A, 411, L299
Kobayashi, S., Ryde, F., & MacFadyen, A. 2002, ApJ, 577, 302
Kocevski, D., Ryde, F., & Liang, E. 2003, ApJ, 596, 389
Lazzati, D. 2002, MNRAS, 337, 1426
Liang, E. P. 1997, ApJ, 491, L15
Liang, E. P., & Kargatis, V. E. 1996, Nature, 381, 495

Lloyd, N., & Petrosian, V. 2000, ApJ, 543, 722
Lyutikov, M., & Blackman, E. G. 2001, MNRAS, 321, 177
MacFadyen, A. I., & Woosley, S. E. 1999, ApJ, 524, 262
Mereghetti, S., Götz, D., Borkowski, J., Walter, R., & Pedersen, H. 2003, A&A, 411, L291
Panaitescu, A., & Kumar, P. 2001, ApJ, 554, 667
Panaitescu, A., & Mészáros, P. 2000, ApJ, 544, L17
Rees, M. J., & Mészáros, P. 1992, MNRAS, 258, 41
Reichart, D. E., Lamb, D. Q., Fenimore, E. E., et al. 2001, ApJ, 552, 57
Ryde, F. 1999, ASP Conf. Proc., 190, 103
Ryde, F., Kocevski, D., & Liang, E. 2003, in Gamma-Ray Bursts and Afterglow Astronomy 2001, ed. G. R. Ricker, & R. K. Vanderspek (New York: AIP), AIP Conf. Proc., 662, 286
Ryde, F., & Petrosian, V. 2002, ApJ, 578, 290
Ryde, F., & Svensson, R. 2000, ApJ, 529, L13
Stern, B., Poutanen, J., & Svensson, R. 1999, ApJ, 510, 312
Tavani, M. 1996, ApJ, 466, 768
Winkler, C., Courvoisier, T. J.-L., Di Cocco, G., et al. 2003, A&A, 411, L1
Zhang, B., & Mészáros, P. 2003, ApJ, 581, 1236